Advanced Pogo Stability Analysis for Liquid Rockets

Bohdan W. Oppenheim* and Sheldon Rubin†

The Aerospace Corporation, El Segundo, California 90245

An advanced modeling method for determining engine-coupled Pogo oscillation modes, with general applicability to any liquid rocket vehicle, is presented. The modes result from interaction of structural vibrations with pressure and flow oscillations in the liquid propulsion system. A time-invariant linearized mathematical model of the system is developed for a selected flight time. Perturbations of the propulsion system are modeled using finite element representations for its physical elements (such as flow duct, pump, accumulator, and thrust chamber), each of which undergoes structural motion described in terms of the vibration modes of the overall vehicle. The structural modes, developed in a separate analysis, are determined with the fluids frozen in place in the feedlines and engines and involve motions of the propulsion elements. The system equations are written in a homogeneous second-order matrix form in the Laplace domain, yielding coefficient matrices that are all complex, unsymmetric, and singular. The major advances are 1) rigorous treatment of arbitrary translational motions of the vessels through which the fluids flow, including all forces (pressure area, inertial, and momentum) that react on the structural system, and 2) a powerful numerical eigensolver that yields eigenvalues and eigenvectors directly, without requiring elimination of dependent fluid state variables (pressure and flows).

Nomenclature

A, A_t = cross-sectional area, nozzle throat area, L^2
$[A]$ = state matrix in eigenvalue problem
a, a^* = acoustic speed in a flexible, rigid duct, LT^{-1}
$[B]$ = system damping matrix
C = compliance (propellant weight change within a container per unit pressure change), L^2
C_f = thrust coefficient, −
C^* = characteristic velocity, LT^{-1}
D = diameter of a duct, L
E = Young's modulus of duct wall material, FL^{-2}
$\bar{F}$ = force vector, F
g = standard gravitational acceleration, LT^{-2}
$\bar{H}$ = head vector from inlet to outlet node of an element (directional components are H_x, H_y, and H_z), L
I = inertance, $L^{-2}T^2$
i = imaginary unit $(-1)^{1/2}$
K = stiffness given by $1/C$, L^{-2}
$[K]$ = system stiffness matrix
ℓ, L = position coordinate along a duct, length along a duct, L
$[M]$ = system mass matrix
M_n = modal mass of nth structural mode, M
MR = mixture ratio, −
m = mass, M
$\bar{m}$ = momentum vector, MLT^{-1}
$m + 1$ = pump dynamic gain, −
N_C, N_M, N_N, N_S = number of thrust chambers, structural modes, propulsion system nodes, and state variables
$\bar{N}_i$ = unit vector in flow direction at node i
$[P]$ = matrix coefficient of state velocity vector in first-order state equation

p, P_s = static pressure perturbation, steady pressure, FL^{-2}
q_n = modal displacement of nth structural mode, L
R, R_s = linearized resistance for flow perturbation, TL^{-2}, steady flow resistance, $F^{-1}L^{-2}T^2$
R_{co}, R_{cf} = linearized combustion resistance for oxidizer, fuel flow perturbation, TL^{-2}
$\bar{r}$ = structural displacement vector, L
$s, \tilde{s}$ = Laplace variable or complex frequency $\sigma + i\Omega$, eigenvalue of system eigenmode, T^{-1}
t = duct wall thickness, L, or time, T
u_a, u = absolute, relative displacement perturbation of fluid in flow direction, L
v, V_s = volume perturbation; mean volume, L^3
$\{\tilde{v}\}$ = eigenvector of system eigenmode
w, W_s = weight displacement perturbation, steady weight displacement, F
$\{y\}$ = state vector in first-order state equation
α = mass flow gain factor for a pump, T
β_n = modal pressure at a tank outlet in the nth structural mode, $FL^{-3}T^2$
$\zeta_n, \tilde{\zeta}$ = fraction of critical damping of nth structural mode, system eigenmode, −
η = parameter set to zero to decouple structure, oxidizer, and fuel systems from each other; otherwise $\eta = 1$
θ = phase shift of the structural modes, −
ρ, ρ_w = mass density, ML^{-3}, weight density, FL^{-3}
$\sigma, \tilde{\sigma}$ = real part of complex frequency, system eigenvalue, T^{-1}
τ_c = combustion time lag, T
$\bar{\phi}_{ni}$ = vector of modal displacement in nth structural mode for ith propulsion element (elements are $\bar{\phi}_{nix}, \bar{\phi}_{niy}, \bar{\phi}_{niz}$)
$\Omega, \tilde{\Omega}$ = imaginary part of complex frequency, system eigenfrequency, T^{-1}
ω_n = circular natural frequency of nth structural mode, T^{-1}
$\tilde{\omega}$ = circular natural frequency of a system mode, T^{-1}

Units are denoted by L for length, F for force, M for mass, T for time, and − for dimensionless.

Subscripts

f = fuel
i,j,k,ℓ,m = node indices
n = structural mode index
o = oxidizer
s = steady or mean value

I. Introduction

Pogo Phenomenon

THE phenomenon of self-excited vibrations of liquid propellant rockets, nicknamed "Pogo" after the jumping stick, has been widely recognized ever since its occurrence on Thor/Agena and Titan II vehicles beginning in the 1960-1962 period. Engine-coupled Pogo is caused by a dynamic instability arising from interaction of vehicle structural dynamics, principally with thrust oscillation of the liquid propulsion system. (A rare form of Pogo, called ullage-coupled Pogo,[1] which does not depend on coupling with thrust oscillation, is not addressed in this paper.) In a classical occurrence, axial periodic vibrations of the overall vehicle have been observed to initiate spontaneously, grow slowly, and then gradually disappear, as depicted in Fig. 1. The slowly changing steady-state characteristics of the coupled Pogo system can give rise to one or more periods of instability during a flight. Occurrences have been in the frequency range from 5 to 120 Hz, the frequency closely matching that of the vehicle structural mode principally involved, with peak vibration amplitudes (zero to peak) reaching from a few tenths of a g to as high as 34 g, and with a duration of the instability of up to 30 s.

The closed-loop process can be viewed as follows: random pressure oscillations in the propulsion system (principally in the thrust chamber) produce vibrations of the vehicle structural modes, which in turn cause pressure oscillations. Alternatively, random vibrations of the vehicle structure produce oscillations in the fluid modes of the propulsion system, which in turn cause structural vibrations principally via thrust. Neither the propulsion system nor the structural system are the "cause"; it is the system interaction that is at the root of the process. Instability will occur during a period of flight when the process is self-reinforcing, causing system vibrations to diverge until nonlinearities produce a limit-cycle behavior. Elimination of such instability has been typically achieved by introducing a hydraulic accumulator device (often called a Pogo suppressor) at one or more appropriate locations within the propellant flow paths.[1] The accumulator causes separation of the critical resonance frequencies of the structural and propulsion systems and thus achieves the desired decoupling.

The Pogo phenomenon has been dealt with extensively. Reference 1, a monograph on Pogo, recommends practices and criteria for mathematical modeling, preflight testing, stability analysis, corrective devices or modifications, and flight evaluation. It contains an extensive bibliography that is not repeated here. An early treatment of Pogo modeling dealing with purely axial vibrations of a vehicle was presented in Ref. 2. It also contains an approximate stability estimation technique to help guide computer studies. That modeling was used to quantify the effectiveness of the accumulators that eliminated Pogo from the Gemini launch vehicle, the first successful demonstration of Pogo stabilization.

Analytical Approach

Pogo stability is analyzed at each of a series of flight times using a time-invariant, linearized mathematical model of the coupled system. The model yields the frequency, damping, and mode shape of all modes of free oscillation of the coupled system. Time-invariant analysis is justified by the relative slowness of the changes in system dynamic characteristics, occurring due to propellant depletion and changes in engine operating conditions. A series of analyses can be performed to investigate the effect of parametric variation (such as degree of pump cavitation or time of flight) and a root-locus diagram generated.

The stability modeling is divided into three tasks. The first involves the modeling and computation of the three-dimensional structural modes of vibration of the overall vehicle, for the various times of flight for which Pogo stability analysis is to be performed. Two constraints are imposed: 1) the main propellant tanks of the vehicle are hydroelastically modeled with the tanks closed at each outlet, and 2) each propulsion
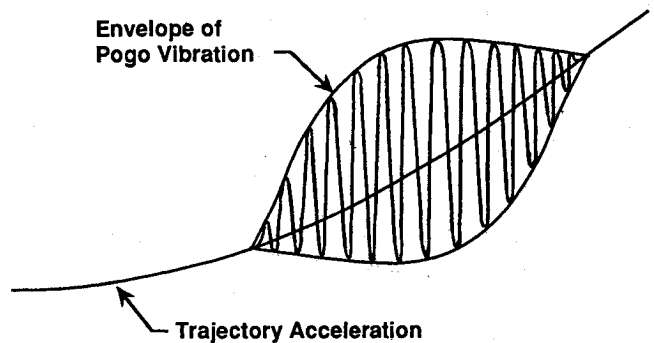

Fig. 1 Typical occurrence of Pogo vibration.

element (ducting and engine components) is modeled as if its contained propellant is frozen in place. Each resulting structural mode shape provides the translational motions of the propulsion elements, as well as the pressure per unit modal acceleration at each outlet from a main propellant tank. Modes are then selected for input to the Pogo model described in the remainder of this paper.

The second task involves the modeling of the propulsion system using the elements described in Sec. II, which characterize flow and combustion dynamics in the presence of arbitrary structural translations. The element modeling is implemented using the finite element technique. The propulsion system model of any liquid rocket is easily assembled from building blocks representing various hardware elements, including a tank outlet, compressible and incompressible ducts, pump, bellows, junction, accumulator, and thrust chamber. Section II describes the modeling of these elements. Section III presents a rigorous treatment of the propulsion system forces acting on the vehicle structural modes, including pressure-area forces, change-of-momentum forces, and inertial forces appropriate to the frozen fluid constraint on the structural modes.

The final task is to calculate the complex eigensolutions for the coupled structure/propulsion system to yield frequency and damping of the system modes and their associated complex mode shapes.

The latter two tasks have been implemented as a general-purpose computer program. The input includes the structural modes and assemblage of the propulsion system elements. The tabulated and graphical output of system modes includes a complete set of state variables (pressures, flows, and structural mode displacements). Section IV describes a powerful eigensolver which permits the solution of the system equations assembled into a second-order matrix set having singular coefficient matrices. The solution is in direct contrast to previous practice at The Aerospace Corporation that required hand manipulation to eliminate variables to achieve an invertible system mass matrix.

A typical Pogo analysis requires that a series of parametric variations in the system model be examined. The program is conducive to implementation of the variations as a sequence of cases and to review of graphical displays of system roots and mode shapes for each case, as well as the locus of selected roots for the variations analyzed.

Major Advances

The present finite element type of modeling approach is somewhat similar to that of Ref. 3, which was developed as a general-purpose Pogo computer program offering a significant degree of automation. The computer program developed using the model described here has more powerful elements for building the propulsion system model including arbitrarily oriented translational motions of the fluid vessels, a rigorous treatment of the flow-induced forces acting on the structure, and a capability to implement a phase shift stability criterion. The program described in Ref. 3 provides only system eigen-

values (roots) and open-loop complex eigenvectors (mode shapes), whereas the work described here provides the roots and associated mode shapes (closed loop) important for gaining insight into system behavior, as well as enabling quantitative correlation with the relative amplitude and phase relationships of pressures and accelerations experimentally determined from flight and ground test data.

II. Propulsion System

Model Elements

The dynamic behavior of perturbations of the propulsion system is modeled by assembly of eight types of elements. These are an incompressible duct, a compressible duct, a flow junction, a bellows, an accumulator, a tank outlet, a pump, and a thrust chamber. Each element has from one to three nodes for interconnection to other elements. Table 1 summarizes the element characteristics in the Laplace domain, including the forces generated by the element to excite the structural modes of the system as described in Sec. III. The propulsion system model is assembled by connecting elements node to node. The node numbering is arbitrary, subject only to a requirement that at each element connection a common node is shared.

Each element type is characterized by a set of linear equations of no higher than second order in time derivative. The equations constitute relationships among the state variables that include perturbational static pressures p (as opposed to total pressures) and corresponding fluid (propellant) relative weight displacements w at the nodes, and also the generalized absolute displacements of the structural modes q. As will be described, required input properties of the fluid are inertance (sometimes called inductance; see Ref. 4), linearized resistance, and volumetric stiffness, as well as geometrical and certain special parameters regarding pump and combustion behavior. The following sections provide the basis for the description of each element in the time domain.

Incompressible Duct

Straight Uniform Duct

As a preliminary to dealing with a general duct geometry, we treat the difference in static pressure along the one-dimensional flow of an incompressible fluid in a straight, uniform area, rigid, moving duct of length L and flow area A (Fig. 2):

$$p_i - p_j = R\dot{w} + I\ddot{w}_a \tag{1}$$

where p_i and p_j are the upstream and downstream pressures, respectively, $\dot{w}$ is the weight flow of the fluid relative to the duct wall, and $\ddot{w}_a$ is the absolute fluid weight acceleration in the flow direction. [In fluid transient modeling there is common use of head (pressure divided by weight density) and volumetric flow as alternative variables to pressure and weight flow (for example, Refs. 4 and 5). This has no impact on the definition of the fluid properties of inertance, resistance, and stiffness.] The term R is a linearization of the drop in mean static pressure ΔP_s that results from the mean turbulent flow $\dot{W}_s$

$$\Delta P_s = R_s \dot{W}_s^2 \tag{2}$$

where R_s is a steady flow resistance that accounts for frictional head loss. For a perturbation in relative flow $\dot{w}$, there results a perturbation in pressure drop given by

$$\Delta p = R\dot{w} \tag{3}$$

where the linearized resistance $R = 2\Delta P_s/\dot{W}_s = 2R_s\dot{W}_s$.

The term $I\ddot{w}_a$ in Eq. (1) is an inertial term stemming from the expression of Newton's second law for the fluid column. If $\ddot{u}$ is the fluid particle absolute acceleration and ρ is the fluid

mass density, the expression of force equals mass times acceleration yields

$$A\Delta p = (\rho AL)\ddot{u}$$

But since by definition the absolute acceleration of the fluid weight $\ddot{w}_a = \rho_w A\ddot{u}$, where $\rho_w = \rho g$ is the fluid weight density,

$$\Delta p = I\ddot{w}_a \tag{4}$$

where $I = L/Ag$ is termed the inertance of the fluid.

If the absolute vector acceleration of the duct wall is $\ddot{r}$, and $\bar{N}$ is the unit vector in the direction of flow, then the fluid relative and absolute weight accelerations are related by

$$\ddot{w} = \ddot{w}_a - \rho_w A\bar{N}\cdot\ddot{r} \tag{5}$$

where the vector dot product $\bar{N}\cdot\ddot{r}$ yields the duct wall acceleration in the direction of flow. Combining Eq. (5) with Eq. (1) yields an expression involving only the relative weight flow and acceleration for the fluid:

$$p_i - p_j = R\dot{w} + I\ddot{w} + \rho L\bar{N}\cdot\ddot{r} \tag{6}$$

The rightmost term in Eq. (6) is the pressure difference due to the acceleration head that would occur along the duct if the fluid were frozen to the moving duct wall. The first two terms on the right of Eq. (6) yield the pressure difference that would occur due to flow perturbation if the duct were motionless.

Incompressible Element

The foregoing is now generalized to one-dimensional incompressible flow along a curved, nonuniform, rigid, moving duct. (The terms in the equations appearing in Table 1 have been organized into coefficients of powers of the Laplace variable, corresponding to the formulation in Sec. III; also the modal force Q_{ni} that appears is derived in Sec. III.) Comparable to Eq. (1)

$$p_i - p_j = R\dot{w} + \int_0^L \bar{N}(\ell)\cdot\ddot{w}_a(\ell)\frac{\mathrm{d}\ell}{A(\ell)g} \tag{7}$$

where again $\dot{w}$ is the fluid weight velocity relative to the wall (independent of position ℓ), and the dot product in the integrand is the absolute fluid weight acceleration at position ℓ in the local flow direction. Corresponding to Eq. (5)

$$\ddot{w} = \bar{N}(\ell)\cdot\ddot{w}_a(\ell) - \rho_w A(\ell)\bar{N}(\ell)\cdot\ddot{r} \tag{8}$$
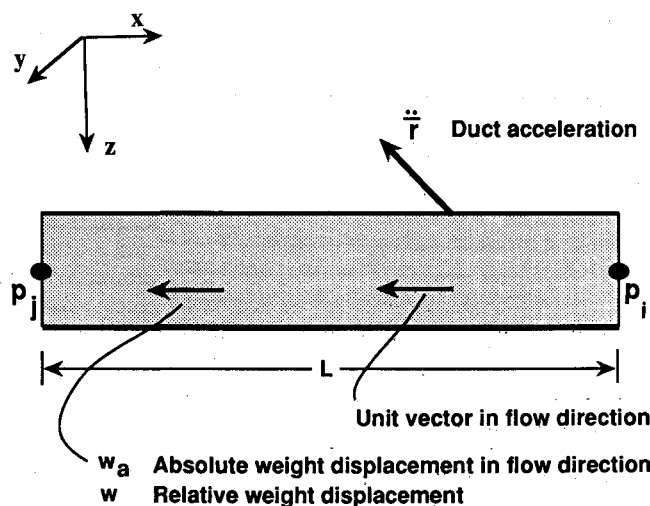

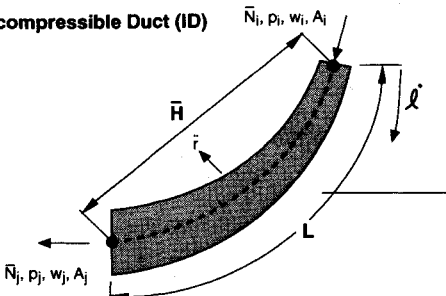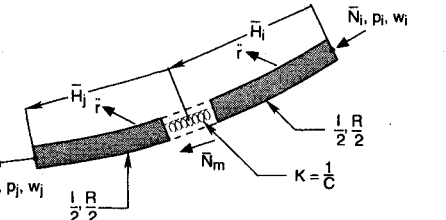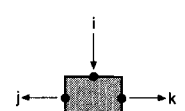Fig. 2 Incompressible fluid in a straight, rigid, uniform, moving duct.

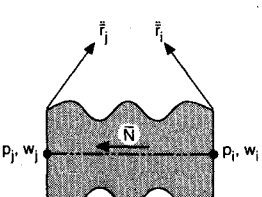**Incompressible Duct (ID)** $\bar{N}_i, p_i, w_i, A_i$

$w_i - w_j = 0$

$$s^2[-Iw_i - \frac{\rho_w}{g}\bar{H}\cdot\bar{r}] + s[-Rw_i] + p_i - p_j = 0$$

$$Q_{ni} = \eta\left\{s^2[-\frac{\bar{H}}{g}\cdot\bar{\phi}_n w_i]\right.$$

$$+ s[\frac{2\dot{W}_s}{\rho_w g}(\frac{\bar{N}_i}{A_i} - \frac{\bar{N}_j}{A_j})\cdot\bar{\phi}_n w_i]$$

$$\left. + A_i\bar{N}_i\cdot\bar{\phi}_n p_i - A_j\bar{N}_j\cdot\bar{\phi}_n p_j\right\}$$

$\bar{N}_j, p_j, w_j, A_j$

Special Case – Local Inertance and/or Resistance: $\bar{H} = \bar{N}_i = \bar{N}_j = 0$

Compressible Duct (D)

$\bar{N}_i, p_i, w_i$

$$s^2[-\frac{I}{2}w_i - \frac{\rho_w}{g}\bar{H}_i\cdot\bar{r}] + s[-\frac{R}{2}w_i] + p_i - Kw_i + Kw_j = 0$$

$$s^2[-\frac{I}{2}w_j + \frac{\rho_w}{g}\bar{H}_j\cdot\bar{r}] + s[+\frac{R}{2}w_i] + p_j - Kw_i + Kw_j = 0$$

$$Q_{ni} = \eta\left\{s^2[-\frac{\bar{H}_i}{g}\cdot\bar{\phi}_n w_i - \frac{\bar{H}_j}{g}\cdot\bar{\phi}_n w_j]\right.$$

$$+ s[\frac{2\dot{W}_s}{\rho_w gA}(\bar{N}_i - \bar{N}_m)\cdot\bar{\phi}_n w_i + \frac{2\dot{W}_s}{\rho_w gA}(\bar{N}_m - \bar{N}_j)\cdot\bar{\phi}_n w_i]$$

$$\left. + A\bar{N}_i\cdot\bar{\phi}_n p_i - A\bar{N}_j\cdot\bar{\phi}_n p_j\right\}$$

$\bar{N}_j, p_j, w_j$ $\frac{I}{2}\frac{R}{2}$ $K = \frac{1}{C}$

Special Case – Local Compliance: $I = R = 0$, $\bar{H}_i = \bar{H}_j = \bar{N}_i = \bar{N}_m = \bar{N}_j = 0$

Then
$$p_i - Kw_i + Kw_j = 0$$
$$p_j - Kw_i + Kw_j = 0$$
$$Q_{ni} = 0$$

Junction (J)

$$p_i - p_j = 0$$
$$p_i - p_k = 0$$
$$w_i - w_j - w_k = 0$$
$$Q_{ni} = 0$$

Bellows (B)

$\bar{r}_j$ $\bar{r}_i$

$\bar{N}$

p_j, w_j p_i, w_i

$$p_i - p_j = 0$$
$$\rho_w A\bar{N}\cdot(\bar{r}_i - \bar{r}_j) + w_i - w_j = 0$$
$$Q_{ni} = 0$$

Note: All structural motions are developed from the structural modes:

$$\bar{r} = \eta\sum_n \bar{\phi}_n q_n, \qquad \bar{\phi}_n \text{ measured at the element}$$

The parameter $\eta = 1$, except $\eta = 0$ when decoupling of the structural and individual propellant system is desired.

Table 1a   Summary of elements

Equations (7) and (8) jointly yield the desired form for the pressure drop, which is a generalization of Eq. (6),

$$p_i - p_j = R\dot{w} + I\ddot{w} + \rho\bar{H}\cdot\ddot{\bar{r}} \tag{9}$$

where the inertance I is given by

$$I = \int_0^L \frac{d\ell}{A(\ell)g}$$

and the head vector $\bar{H}$ denotes the vector distance from the inlet to outlet nodes (nodes geometrically positioned at the centers of the flow areas), where

$$\bar{H} = \int_0^L \bar{N}(\ell)\, d\ell$$

Equation (9) is the basis for representation of an incompressible duct element appearing at the beginning of Table 1, along with the constraint that $w_i = w_j$. A special case of this

Accumulator (A)

$\bar{N}_j, p_j, w_j$ — Gas

$\bar{N}_i, p_i, w_i$

$$s^2\left[-\,Iw_i - \frac{\rho_w}{g}\bar{H}\bullet\bar{r}\right] + s\left[-\,Rw_i\right] + p_i - Kw_i = 0$$

$$Q_{ni} = \eta\left\{s^2\left[-\frac{\bar{H}}{g}\bar{\phi}_n w_i\right] + A_i\bar{N}_i\bullet\bar{\phi}_n p_i - A_i K\bar{N}_j\bullet\bar{\phi}_n w_i\right\}$$

Tank Outlet (T)

Tank

$\bar{N}_i, p_i, w_i$ — Duct

$$s^2\left[Iw_i - \eta\sum_n \beta_n q_n\right] + s\left[Rw_i\right] + p_i = 0$$

$$Q_{ni} = \eta\left\{s^2\left[\frac{\beta_n}{\rho_w}w_i\right] - A\bar{N}\bullet\bar{\phi}_n p_i\right\}$$

Pump (P)

$\bar{N}_i, p_i, w_i$

$\bar{r}$ $\bar{H}$ $\bar{N}_j, p_j, w_j$

$$s^2\left[-Iw_j - \frac{\rho_w}{g}\bar{H}\bullet\bar{r}\right] + s\left[-\,Rw_j\right] + (m+1)p_i - p_j = 0$$

$$s\left[K\alpha w_i\right] - Kw_i + Kw_j + p_i = 0$$

$$Q_{ni} = \eta\left\{s^2\left[-\frac{\bar{H}}{g}\bar{\phi}_n w_j\right] + s\left[\frac{2\dot{W}_s}{\rho_w g}\left(\frac{\bar{N}_i}{A_i} - \frac{\bar{N}_j}{A_j}\right)\bullet\bar{\phi}_n\right]\right.$$
$$\left. + A_i\bar{N}_i\bullet\bar{\phi}_n p_i - A_j\bar{N}_j\bullet\bar{\phi}_n p_j\right\}$$

Thrust Chamber (C)

i - ℓ = oxidizer injector orifices
j - m = fuel injector orifices
ℓ, m = uncoupled chamber pressure nodes
k = chamber pressure node

p_i, w_i p_j, w_j

p_ℓ p_m A_t, (Throat Area)

p_k

$\bar{N}_k$

Two propellant case (as shown):

$$s^2\left[-\,I_i w_i\right] + s\left[-\,R_i w_i\right] + p_i - p_\ell - \eta p_m = 0$$

$$s^2\left[-\,I_j w_j\right] + s\left[-\,R_j w_j\right] + p_j - \eta p_\ell - p_m = 0$$

$$s\left[\tau_c p_\ell - R_{ci}\,w_i\right] + p_\ell = 0$$

$$s\left[\tau_c p_m - R_{cj}\,w_j\right] + p_m = 0$$

$$p_k - p_\ell - p_m = 0$$

One propellant case (j, ℓ, m not present):

$$s^2\left[-\,I_i w_i\right] + s\left[-\,R_i w_i\right] + p_i - p_k = 0$$

$$s\left[\tau_c p_k - R_{ci} w_i\right] + p_k = 0$$

Both cases:

$$Q_{nk} = \eta\left\{-A_t C_f\bar{N}_k\bullet\bar{\phi}_n p_k\right\}$$

Structural Mode (M)

$$s^2\left[M_n q_n\right] + s\left[2\zeta_n\omega_n M_n q_n\right] + M_n\omega_n^2 q_n - \sum_i Q_{ni} = 0 \qquad\qquad n = 1, 2, \ldots, N_m$$

i is the index over all propulsion system elements

Table 1b   Summary of elements

representation with $\bar{H} = 0$ is a local resistance and inertance. This could be used, for example, to model noncavitating flow through an orifice, or through a group of orifices such as an injector, or through a valve.

In a duct with nonuniform area, the steady flow resistance, defined in Eq. (2), accounts for velocity head change as well as frictional loss. The steady pressure drop can be written as the sum of the two effects:

$$\Delta P_s = \Delta P_s\Big|_{\text{friction}} + \frac{\dot{W}_s^2}{2\rho_w g}\left(\frac{1}{A_i^2} - \frac{1}{A_j^2}\right) \qquad (10)$$

where A_i and A_j are the inlet and outlet areas, respectively. The relationships for the linearized resistance R, given after Eq. (3), still apply. Note that if the duct is expanding in area (that is, $A_j > A_i$), the velocity head term will yield a pressure rise (negative pressure drop). If this pressure rise exceeds the frictional pressure drop, the result is a negative linearized resistance.

Fluid Compliance

Consistent with use of weight displacement as the measure of fluid motion, the term compliance (sometimes called capac-

itance) describes the increase in the weight of fluid between inlet and outlet of a container due to a pressure increase. Fluid compressibility (for a liquid, expressed by the inverse of its adiabatic bulk modulus), container elasticity, and presence of gas contribute to compliance. When the fluid region involved is sufficiently small that the pressure perturbation p can be taken to be uniform between nodes i and j, we can characterize the compliance C by

$$C = \frac{w_i - w_j}{p} \qquad (11a)$$

or the fluid stiffness K, where $K = 1/C$, by

$$p = K(w_i - w_j) \qquad (11b)$$

For a uniform, circular duct containing a liquid and no gas, the compliance is

$$C = \rho_w V_s \left[\frac{1}{B} + \frac{D}{Et} \right] \qquad (12)$$

where V_s is the steady (mean) volume of liquid, and B is its bulk modulus, the reciprocal of which is the fractional contraction of the liquid volume, $-\Delta V/V_s$, per unit pressure rise Δp:

$$\frac{1}{B} = -\frac{\Delta V/V_s}{\Delta p} \qquad (13)$$

The quantity D/Et is the fractional volume increase per unit pressure rise due to radial growth of a thin-walled circular duct, assuming that associated axial length change is unconstrained. Empirical and theoretical expressions for volumetric stiffness of various duct configurations can be found in Refs. 4 and 5.

It is also of interest to determine the speed of travel of pressure or flow perturbations along the duct, called the acoustic speed. In a rigid duct, the acoustic speed $a*$ is given by

$$a* = (B/\rho)^{1/2}$$

whereas in a flexible duct the effective acoustic speed a is given by

$$a = \left\{ \rho \left[\frac{1}{B} + \frac{D}{Et} \right] \right\}^{-1/2} = \left(\frac{gV_s}{C} \right)^{1/2} = (gV_sK)^{1/2} \qquad (14)$$

It is also useful to express the stiffness K in terms of the acoustic speed and the steady volume V_s, namely,

$$K = \frac{1}{C} = \frac{a^2}{gV_s} \qquad (15)$$

When the fluid involved is a gas, dynamic perturbations of its volume are taken to behave adiabatically, namely,

$$(P_s + p)(V_s + v)^\gamma = \text{const} \qquad (16)$$

where P_s, V_s and p, v are the steady and perturbational pressure and volume, and γ is the ratio of specific heats of the gas. Retaining first-order perturbational terms,

$$K = \frac{1}{C} = \frac{p}{\rho_w v} = \frac{\gamma P_s}{\rho_w V_s} \qquad (17)$$

where ρ_w is the associated liquid propellant weight density, required because of the definition of compliance and stiffness in terms of the change in weight of propellant between nodes. An equivalent bulk modulus for the gas B_g is given by

$$B_g = \frac{\rho_w V_s}{C} = \gamma P_s \qquad (18)$$

This B_g is an appropriate replacement for B in Eqs. (12) and (14) when the fluid is a gas. For example, the acoustic speed in a gas having a density ρ is given by

$$a = \left(\frac{\gamma P_s}{\rho} \right)^{1/2} \qquad (19)$$

assuming that flexibility of the duct wall contributes negligibly, as is the usual case.

Duct Element

The duct element defined here applies to a low-frequency, one-dimensional representation of compressible flow in a curved, uniform duct. It is patterned after the half-mass, spring, half-mass finite element model for a uniform mechanical system governed by the one-dimensional wave equation (for example, axial vibration of a uniform rod). Such a duct element is depicted in Table 1 with incompressible end portions, each representing half the inertance and resistance of the element, and with the centrally located stiffness representing the total volumetric stiffness of the element. An arbitrary contour of the duct centerline is accommodated via independent head vectors for each end. Allowing each half to have nonuniform area, although easy to do, is inconsistent with the symmetric character of the inertance-resistance properties and is therefore not included as an option for the compressible duct element. Situations that require compressible flow modeling in nonuniform ducts (in an inertance and/or resistance sense) should be given individual consideration and can be modeled by an appropriate combination of incompressible elements and local compliance elements.

Referring to Table 1 for the compressible duct element, applying Eq. (9) to the two end portions and replacing the midpoint pressure p_m using the stiffness relationship from Eq. (11b) yields

$$p_i - \left(\frac{I}{2}\ddot{w}_i + \frac{R}{2}\dot{w}_i + Kw_i \right) + Kw_j - \rho \bar{H}_i \cdot \ddot{r} = 0$$

$$p_j + \left(\frac{I}{2}\ddot{w}_j + \frac{R}{2}\dot{w}_j + Kw_j \right) - Kw_i + \rho \bar{H}_j \cdot \ddot{r} = 0 \qquad (20)$$

Differencing and summing the pair of Eqs. (20) yields another form:

$$p_i - p_j = \frac{I}{2}(\ddot{w}_i + \ddot{w}_j) + \frac{R}{2}(\dot{w}_i + \dot{w}_j) + \rho(\bar{H}_i + \bar{H}_j) \cdot \ddot{r} \qquad (21a)$$

$$p_i + p_j = \frac{I}{2}(\ddot{w}_i - \ddot{w}_j) + \frac{R}{2}(\dot{w}_i - \dot{w}_j) + \rho(\bar{H}_i - \bar{H}_j) \cdot \ddot{r}$$

$$+ 2K(w_i - w_j) \qquad (21b)$$

In this latter form the limiting case of a local fluid compliance is clearly achieved by setting I, R, $\bar{H}_i$, and $\bar{H}_j$ to 0. First, Eq. (21a) yields $p_i - p_j = 0$ and then Eq. (21b) yields $p_i = K(w_i - w_j)$, which produces the result in Eq. (11b). The form in Eqs. (20), numerically equivalent to that in Eqs. (21), is implemented as the compressible duct element (Table 1).

The use of the foregoing duct element for compressible flow must be restricted to a small fraction of a wavelength to justify its lumped-parameter form. It is recommended that use be restricted to duct lengths that do not exceed one-tenth of a wavelength over the frequency range of interest. The criterion for length of a duct element is then

$$L \le \frac{a}{10f_u} \qquad (22)$$

where f_u is the highest frequency of interest in Hz, and a is the effective acoustic speed given by Eq. (14) for a liquid or by Eq. (19) for a gas. Reference 6 contains a detailed analysis of

a) 1 Inlet, 2 Outlets

b) 2 Inlets, 1 Outlet

c) Combinations:

1 Inlet, 3 Outlets

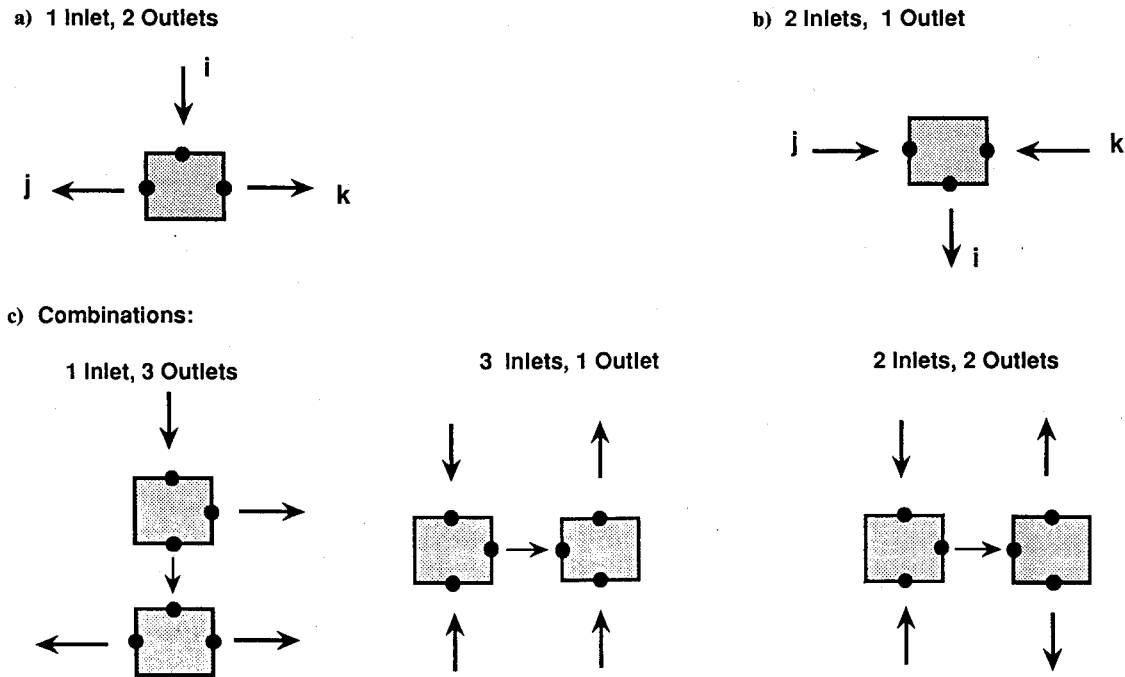**3 Inlets, 1 Outlet**

2 Inlets, 2 Outlets

Fig. 3 Junction element schematic and combinations.

various modeling forms for uniform ducts and the resulting errors in various frequency response functions from an exact modeling. The form used here is chosen because of the ease of physical interpretation, even though other forms can handle larger fractions of a wavelength.

Junction Element

The junction element is an idealized joiner of three flow streams. The element is assumed to have zero length and is devoid of pressure loss, inertance, and compliance. The first possibility is one inlet denoted by i and two outlet nodes denoted by j and k, as depicted by the schematic of Fig. 3a. Alternatively, there may be two inlet nodes j and k and one outlet node i as shown in Fig. 3b. The condition that the perturbation pressure is the same at all three nodes yields

$$p_i = p_j = p_k \tag{23}$$

The incompressibility condition yields

$$w_i = w_j + w_k \tag{24}$$

The form of these equations used for the system equations is shown in Table 1.

Any junction involving more than three flows can be represented by cascading multiple junction elements, as shown in Fig. 3c. For one inlet, each outlet beyond two requires an additional junction. Also, multiple inputs and a single output are created by simply reversing the directions of the flows.

Bellows Element

An axially compliant bellows device is often used in feed-lines to facilitate relative structural motions. This is typically accomplished with a bellows device whose length is of the order of one diameter of the duct. A schematic of such a device is shown in Table 1. For modeling purposes, it is assumed that the discontinuity in pipe displacement across the bellows occurs in a vanishingly short distance in the flow direction. Fluid inertance, resistance, and compliance effects in the physical bellows are accounted for in the adjacent elements.

The equations describing the sudden discontinuity in axial pipe motion are

$$p_i = p_j \tag{25a}$$

$$w_i + \rho_w A \bar{N} \cdot \ddot{r}_i = w_j + \rho_w A \bar{N} \cdot \ddot{r}_j \tag{25b}$$

Equation (25b) expresses the continuity in absolute weight displacement of the fluid across the bellows element. See Table 1 for the model of an idealized bellows element.

Accumulator Element

An accumulator is a type of a device commonly used to suppress Pogo instability. It contains a volume of gas that acts as a soft volumetric spring, intended to shift hydraulic frequencies so as to reduce the dynamic coupling between the propulsion system and vehicle structural modes of vibration. Either the gas can be in direct contact with the propellant (particularly true for cryogenic propellants), or it can be contained within a bladder or bellows that provides low stiffness compared with that of the enclosed gas. A number of accumulator types are depicted in Ref. 1.

A schematic representation of an accumulator as a branch device from a flow duct is shown in Table 1. The inlet node of the accumulator is denoted i. The path to the gas volume is taken to be incompressible. The node j is at the center of the fluid-gas interface surface. (Note that if the accumulator is axially symmetric about the flow duct, the node j will be located on the duct centerline.) Any bladder or bellows surrounding the gas is assumed to have zero mass. If this is not true, such mass can be accounted for by adding an equivalent inertance to the path from i to j. From Eq. (9)

$$p_i - p_j = R \dot{w}_i + I \ddot{w}_i + \rho \bar{H} \cdot \ddot{r} \tag{26}$$

where the head vector $\bar{H}$ originates at the center of the duct (to be consistent with treatment of head along the duct) and $\ddot{r}$ is the accumulator housing acceleration.

The gas pressure p_j is related to gas volume change, which is dictated by the inlet relative weight displacement w_i of liquid. From the relationship in Eq. (11b),

$$p_j = K w_i \tag{27}$$

where K is the gas stiffness given by Eq. (17). If the gas is contained within a bellows or bladder that has nonnegligible stiffness, that stiffness must be included within the parameter K. Combining Eqs. (26) and (27), the final result is written as

$$p_i - (I\ddot{w}_i + R\dot{w}_i + Kw_i) - \rho\bar{H}\cdot\ddot{r} = 0 \tag{28}$$

It is often necessary to express the mean volume of the gas V_s in terms of the conditions under which the gas originally was placed into the accumulator (called precharge). Let P_o, V_o, and T_o be the precharge pressure, volume, and absolute temperature, and let T_s be the operating temperature of the gas. Perfect gas behavior requires that

$$\frac{P_o V_o}{T_o} = \frac{P_s V_s}{T_s} \tag{29}$$

and K can then be written in the useful form

$$K = \frac{1}{C} = \frac{\gamma P_s^2}{\rho_w P_o V_o}\frac{T_o}{T_s} \tag{30}$$

Tank Outlet Element

As mentioned in Sec. I, one of the constraint conditions for the structural modes is closure of the main propellant tanks. As depicted in Table 1, the dotted interface at a tank outlet indicates the position of such a closure denoted by i. The tank outlet element describes the relationship of the perturbational pressure at point i to the acceleration of the structural modes, as well as the effect of perturbational flow from the tank (derived in Ref. 6):

$$p_i = \sum_n \beta_{ni}\ddot{q}_n - R\dot{w}_i - I\ddot{w}_i \tag{31}$$

The first term on the right is the contribution of the structural modes in the absence of relative flow, where β_{ni} is the modal tank-outlet pressure per unit acceleration of the nth mode $\ddot{q}_n$. The second term, involving the resistance R, reflects the linearization of frictional and velocity head effects in the steady flow from the tank interior to the point i as described by Eq. (10). The inertance I in the last term should be viewed as the ratio of perturbational pressure to weight acceleration (into the tank) that would exist if a piston were oscillating at node i and steady flow were absent. The calculation of I would use the integral expression stated for Eq. (9). The result in Eq. (31) is a generalization of Eq. (A-23) in Appendix A of Ref. 6 because there the flow resistance was neglected.

Pump Element

Modeling of a pump (Table 1) can be subdivided into two parts. The first deals with the bubbly (cavitating) flow region in the inducer (leading portion of the blading) as discussed in Ref. 7. The second part describes the subsequent incompressible flow to the outlet (pump discharge) and involves linearization of certain performance characteristics.

The production of cavitation bubbles has two effects described by the following equation:

$$w_i - w_j = C_b p_i + \alpha\dot{w}_i \tag{32}$$

where C_b is called the "cavitation compliance" and α is called the "mass flow gain factor."[7] The compliance term stems from the volumetric perturbation of the bubbles owing to inlet pressure perturbation, an effect long recognized as crucial to the modeling of Pogo.[1] The coefficient α (corresponds to the factor M in Ref. 7), inferred on the basis of experimental transfer function data for a cavitating inducer, stems from an assumed proportionality between the angle-of-attack perturbation at the inducer inlet and the perturbation in rate of production of bubbles.

The description of the incompressible flow beyond the bubbly region can be written

$$p_i - p_j = I\ddot{w}_j + \rho\bar{H}\cdot\ddot{r} - \Delta p \tag{33}$$

where the first two right-hand terms characterize fluid inertia effects just as in Eq. (9). The term Δp is visualized as the result of linearization of two nonlinear steady-state pump performance characteristics, namely, head rise vs inlet pressure at constant flow and head rise vs flow at constant inlet pressure.[1,2] These linearizations yield

$$\Delta p = m p_i - R_p \dot{w}_j \tag{34}$$

where

$$m = \frac{\partial(P_{sj} - P_{si})}{\partial P_{si}} \quad \text{and} \quad -R_p = \frac{\partial(P_{sj} - P_{si})}{\partial\dot{W}_s}$$

where P_{si} and P_{sj} are the steady inlet and outlet (suction and discharge) pressures. The combination of Eqs. (32-34) yields the pair of equations for a pump in the following form:

$$p_j = (m + 1)p_i - R_p\dot{w}_j - I\ddot{w}_j - \rho\bar{H}\cdot\ddot{r} \tag{35a}$$

$$p_i = K_b(w_i - w_j) - \alpha K_b\dot{w}_i \tag{35b}$$

where $K_b = 1/C_b$. It should be pointed out that the quantity $m + 1$, often called "pump gain," should ideally be obtained experimentally from perturbational oscillation test data rather than from the slope of the steady-state head rise vs inlet pressure. Limited data suggest that the latter basis may be unreliable.

Thrust Chamber Element

The thrust chamber element (Table 1) includes the oxidizer and fuel injector orifices, treated as equivalent incompressible ducts, as well as the combustion chamber itself. The fluids upstream of the orifices are typically treated as compressible duct elements, such as an injector cavity (manifold) or regenerative cooling tubes.

Under steady flow conditions the chamber pressure P_c is proportional to the sum of the weight flows of the oxidizer and fuel

$$P_c = \frac{C^*}{A_t g}(\dot{W}_{so} + \dot{W}_{sf}) \tag{36}$$

The C^* is primarily a function of the mixture ratio MR, which is defined as the ratio of the steady oxidizer and fuel weight flows:

$$MR = \frac{\dot{W}_{so}}{\dot{W}_{sf}} \tag{37}$$

The thrust chamber element describes the oxidizer and fuel flow perturbation $\dot{w}_o$ and $\dot{w}_f$ through the injector orifices and their transition into chamber pressure perturbation. The combustion relationship employed is identical, except for notational differences, to that first derived in Ref. 2:

$$\tau_c\dot{p}_c + p_c = R_{co}\dot{w}_o + R_{cf}\dot{w}_f \tag{38}$$

These resistance-like coefficients are derived from a linearization of the characteristic velocity C^* vs mixture ratio characteristic at the steady operating point of the combustion process, namely,

$$R_{co} = [C_s^* + (1 + MR_s)](dC_s^*/dMR_s)A_t g \tag{39a}$$

$$R_{cf} = [C_s^* - MR_s(1 + MR_s)](dC_s^*/dMR_s)A_t g \tag{39b}$$

where C_s^* and MR_s are the characteristic velocity and mixture ratio for the steady condition being perturbed.

The combustion time lag τ_c results from a low-frequency approximation of the time required for the perturbation of incoming flows to produce a perturbation in chamber pressure. A more precise description involves an individual delay time τ_d for each propellant that accounts for its flight within the chamber and its vaporization and a residence time τ_r(common to both propellants) that accounts for mixing and reaction before expulsion from the chamber.[8] This viewpoint yields the combustion relationship

$$\tau_r \dot{p}_c(t) + p_c(t) = R_{co}\dot{w}_o(t - \tau_{do}) + R_{cf}\dot{w}_f(t - \tau_{df}) \qquad (40)$$

When the times τ_{do} and τ_{df} are not too different, and also when the sum of τ_r and the average delay time τ_d is less than one-tenth of the period of the highest frequency structural mode that may be significant for Pogo stability, the simple time lag representation of Eq. (38) is justified, where $\tau_c = \tau_r + (\tau_{do} + \tau_{df})/2$. If this is not justified, Eq. (40) can be transformed to the Laplace domain and converted into a suitable approximation that is valid over the frequency range of interest. An example of this is contained in Appendix D of Ref. 9.

Oxidizer and fuel flow entering the chamber emanate from their injector orifices, described by their resistance and inertance. The pressure drops across the orifices are included in the thrust chamber element. From Eqs. (1) or (9),

$$p_{\text{inj}o} - p_c = R_{\text{inj}o}\dot{w}_o + I_{\text{inj}o}\ddot{w}_o \qquad (41a)$$

$$p_{\text{inj}f} - p_c = R_{\text{inj}f}\dot{w}_f + I_{\text{inj}f}\ddot{w}_f \qquad (41b)$$

where the subscripts inj$o$ and inj$f$ denote oxidizer and fuel injector orifice quantities, respectively.

For diagnostic and program checkout purposes, it is useful to designate the oxidizer and fuel flow contributions to the chamber pressure separately, replacing Eq. (38) by

$$p_c = p_{co} + p_{cf} \qquad (42a)$$

$$\tau_c \dot{p}_{co} + p_{co} = R_{co}\dot{w}_o \qquad (42b)$$

$$\tau_c \dot{p}_{cf} + p_{cf} = R_{cf}\dot{w}_f \qquad (42c)$$

It is then possible to use a parameter η to achieve a decoupling of the oxidizer and fuel interactions through chamber pressure, namely, Eqs. (41) are rewritten as

$$p_{\text{inj}o} - p_{co} - \eta p_{cf} = R_{\text{inj}o}\dot{w}_o + I_{\text{inj}o}\ddot{w}_o \qquad (43a)$$

$$p_{\text{inj}f} - p_{cf} - \eta p_{co} = R_{\text{inj}f}\dot{w}_f + I_{\text{inj}f}\ddot{w}_f \qquad (43b)$$

When $\eta = 1$, the proper interaction occurs in the combustion chamber, whereas $\eta = 0$ produces decoupling by selective removal of the other propellant flow into the chamber.

See Table 1 for the thrust chamber element. The subscripts i, j, k, ℓ, and m appear with the following relation to those used in the foregoing equations: i and j are used for the oxidizer and fuel injector quantities (that is, inj$o \rightarrow i$ and inj$f \rightarrow j$), and the chamber pressures p_c, p_{co}, and p_{cf} are replaced by p_k, p_ℓ, and p_m, respectively.

At times the effect of only one propellant is modeled. It is then adequate to retain one injector node (say i) and node k, and the equations reduce to the two shown in Table 1 for this case.

III. Structural System

The vehicle structural system is defined to include the hydroelastic dynamic behavior of the main propellant tanks with a boundary condition of zero outflow and to include the inertial effect of "frozen in place" propellant in feedlines and engine components. Free-free, real normal modes of vibration are determined in a separate computer program, possibly followed by a selection process to identify the modes most significant for Pogo coupling. The modes are then input to the Pogo program.

Equations of Motion

A physical displacement vector at point i on the structure at time t, $\bar{r}_i(t)$, is expressed in terms of a summation of contributions $\bar{r}_{ni}(t)$ from the individual structural modes whose number is designated N_M:

$$\bar{r}_i(t) = \sum_{n=1}^{N_M} \bar{r}_{ni}(t), \qquad \bar{r}_{ni}(t) = \bar{\phi}_{ni}q_n(t) \qquad (44)$$

and where $\bar{\phi}_{ni}$ is the vector mode shape at point i, and $q_n(t)$ is the modal displacement (often referred to as generalized displacement) at time t, all written for mode n. The equation of motion for mode n is written as

$$M_n[\ddot{q}_n(t) + 2\zeta_n \omega_n \dot{q}_n(t) + \omega_n^2 q_n(t)] = Q_n(t)e^{i\theta} \qquad (45)$$

where ω_n, ζ_n, and M_n are the modal circular natural frequency, fraction of critical damping, and mass, and θ is a phase shift imposed on all of the structural modes. This phase shift is used to implement a phase shift stability criterion as defined in Ref. 1. The modal force at time t, $Q_n(t)$ (often referred to as generalized force), results from a summation of contributions from all of the elements of the propulsion system:

$$Q_n(t) = \sum_i Q_{ni}(t) = \sum_i \bar{F}_i(t) \cdot \bar{\phi}_{ni} \qquad (46)$$

where $\bar{F}_i(t)$ is the vector force at time t produced by the ith element and $\bar{\phi}_{ni}$ is the vector modal deflection of the ith element. The forces $\bar{F}_i$ are due to fluid flow, combustion, and removal of fictitious forces developed because of the constraint that fluids are frozen to their container for determination of the structural modes. All of these forces are derived in the next section.

Forces Produced by Propulsion Elements

With the exception of the junction and bellows elements, flow perturbations result in forces acting on the structural system. These forces are now identified.

Incompressible Duct Element

Consider the incompressible flow of fluid through the curved, nonuniform area duct depicted in Table 1 for the incompressible duct. The pressure and flow are taken as uniform over each cross section. The basis for the derivation of forces is the vector translational momentum equation for an accelerating volume of fluid.[10] The integrated external force $\bar{F}_A$ acting on the surface of the fluid volume can be written

$$\bar{F}_A = \frac{d\bar{m}}{dt} + \int_A \rho \bar{U}_a(\dot{U} \cdot d\bar{A}) \qquad (47)$$

In other words, the resultant vector force equals the rate of change of the vector momentum $\bar{m}$ of the fluid within the volume plus the net outflow of vector momentum from the volume (expressed by an integral over the entire surface area of the fluid). The quantities $\bar{U}_a$ and $\dot{U}$ are the total (steady plus perturbation) fluid particle velocities in an absolute frame of reference and in a frame relative to the moving rigid duct, respectively. The quantity $d\bar{A}$ is an elemental surface area vectored along an outward normal to the fluid surface.

The contained fluid momentum for the duct in Fig. 2 is

$$\bar{m} = \int_0^L \rho A(\ell)\bar{U}_a(\ell) \, d\ell \qquad (48)$$

where $\dot{U}_a(\ell)$ is the average absolute velocity over the cross-sectional area $A(\ell)$ at position ℓ. The velocity of the fluid relative to the duct is

$$\dot{U}(\ell) = \dot{U}_a(\ell) - \dot{r} = \frac{\dot{W}}{\rho_w A(\ell)} \bar{N}(\ell) \qquad (49)$$

where $\dot{r}$ is the vector translational velocity of the rigid duct wall, $\dot{W}$ is the total relative weight flow (steady part $\dot{W}_s$ plus perturbation $\dot{w}$), and $\bar{N}(\ell)$ is a unit vector in the flow direction at ℓ. Using Eqs. (48) and (49), the momentum vector can then be written as

$$\bar{m} = \frac{\dot{W}}{g} \bar{H} + m_f \dot{r} \qquad (50)$$

where m_f is the mass of contained fluid, and $\bar{H}$, as before, is the head vector from the center of the inlet cross section to the center of the outlet cross section. Since the duct wall is limited to translation, $\bar{H}$ is constant and therefore

$$\frac{d\bar{m}}{dt} = \frac{\dot{w}}{g} \bar{H} + m_f \ddot{r} \qquad (51)$$

The first term accounts for accelerating flow relative to the duct (perturbational flow only since there is no acceleration of the relative steady flow) and the second for the inertia effect of the fluid if frozen to the duct wall.

The result of the application of the momentum outflow integral in Eq. (47) to the duct is a contribution at the inlet and one at the outlet. The inlet contribution to outflow is written as

$$\rho \left(\frac{\dot{W}}{\rho_w A_i} \bar{N}_i + \dot{r} \right) \left(-\frac{\dot{W}}{\rho_w A_i} A_i \right)$$

where the first expression in parentheses is the absolute velocity $\bar{U}_a$ using Eq. (49), followed in the second expression in parentheses by the replacement of $\dot{U} \cdot d\bar{A}$ in terms of relative weight flow with the negative sign indicating inflow (negative outflow). Similarly, the contribution at the outlet is

$$\rho \left(\frac{\dot{W}}{\rho_w A_j} \bar{N}_j + \dot{r} \right) \left(\frac{\dot{W}}{\rho_w A_j} A_j \right)$$

The net result is

$$\int_A \rho \dot{U}_a (\dot{U} \cdot d\bar{A}) = \left(\frac{\dot{W}^2}{\rho_w g} \right) \left(\frac{\bar{N}_j}{A_j} - \frac{\bar{N}_i}{A_i} \right)$$

Retaining only first-order perturbations,

$$\int_A \rho \dot{U}_a (\dot{U} \cdot d\bar{A}) = \frac{2\dot{W}_s \dot{w}}{\rho_w g} \left(\frac{\bar{N}_j}{A_j} - \frac{\bar{N}_i}{A_i} \right) \qquad (52)$$

Inserting Eqs. (51) and (52) into Eq. (47), the net force perturbation on the fluid surface $\bar{F}_f$ is

$$\bar{F}_f = \frac{\dot{w}}{g} \bar{H} + m_f \ddot{r} + \frac{2\dot{W}_s \dot{w}}{\rho_w g} \left(\frac{\bar{N}_j}{A_j} - \frac{\bar{N}_i}{A_i} \right) \qquad (53)$$

This force must also equal the pressure-area forces on the two end cross sections of the fluid plus the force that the duct wall imparts to the fluid (negative of the force $\bar{F}$ that the fluid imparts to the duct). Therefore,

$$\bar{F}_f = p_i A_i \bar{N}_i - p_j A_j \bar{N}_j - \bar{F}$$

yielding, with the removal of the $m_f \ddot{r}$ term,

$$\bar{F} = p_i A_i \bar{N}_i - p_j A_j \bar{N}_j - \frac{\dot{w}}{g} \bar{H} + \frac{2\dot{W}_s \dot{w}}{\rho_w g} \left(\frac{\bar{N}_i}{A_i} - \frac{\bar{N}_j}{A_j} \right) \qquad (54)$$

An $m_f \ddot{r}$ term has been eliminated since the inertial effect of the frozen-in-place fluid has already been taken into account in the structural system modeling.

For the special case of a uniform, straight duct $(A_i = A_j = A$, $\bar{N}_i = \bar{N}_j = \bar{N}$, $\bar{H} = L\bar{N})$, the force on the duct is

$$\bar{F} = \left[(p_i - p_j)A - \dot{w}\frac{L}{g} \right] \bar{N}$$

Inserting the expression for $p_i - p_j$ from Eq. (6) and replacing I by L/Ag, we obtain

$$\bar{F} = \dot{w}AR\bar{N} + m_f (\ddot{r} \cdot \bar{N})\bar{N} \qquad (55)$$

The first term is the contribution of friction, and the second term negates the inertial force in the direction of flow for the frozen-in-place fluid assumed for the structural modes. These are intuitively reasonable results.

Compressible Duct Element

The force acting on the structural system due to flow in a compressible duct element (Table 1) results from the application of Eq. (54) to the two incompressible end portions of the model. Since the area is constant, $A_j = A_i$, and letting $\bar{N}_m$ be the unit vector in the flow direction at the midpoint m, the net force on the duct wall is

$$\bar{F} = p_i A_i \bar{N}_i - p_j A_i \bar{N}_j - \frac{\dot{w}_i}{g} \bar{H}_i - \frac{\dot{w}_j}{g} \bar{H}_j + \frac{2\dot{W}_s}{\rho_w g A_i} [(\bar{N}_i - \bar{N}_m)\dot{w}_i$$

$$+ (\bar{N}_m - \bar{N}_j)\dot{w}_j] \qquad (56)$$

Note that for the special case of a local compliance, a special case as discussed following Eqs. (21), there is no resultant force since $p_i = p_j$, $\bar{N}_i = \bar{N}_j = \bar{N}_m$, and $\bar{H}_i = \bar{H}_j = 0$.

Accumulator Element

For the accumulator element (Table 1), the force is that due to the incompressible flow from the center of the duct that feeds the accumulator to the center of the liquid/gas interface at node j. From Eq. (54), using the stiffness relationship of Eq. (27) to eliminate p_j, and noting that there is no steady flow so that $\dot{W}_s = 0$,

$$\bar{F} = p_i A_i \bar{N}_i - w_i A_j K \bar{N}_j - \frac{\dot{w}_i}{g} \bar{H} \qquad (57)$$

Tank Outlet Element

As derived in Ref. 6, the effective modal force acting on the nth structural mode, due to tank outlet conditions at node i, is

$$Q_{ni} = \dot{w}_i \frac{\beta_{ni}}{\rho_w} - p_i A_i \bar{N}_i \cdot \bar{\phi}_{ni} \qquad (58)$$

where, as defined in connection with Eq. (31), β_{ni} is the tank-outlet modal pressure per unit modal acceleration, $\bar{\phi}_{ni}$ is the vector modal deflection, and $\bar{N}_i$ is the unit vector in the flow direction (Table 1). The first term accounts for the effect of the perturbation of flow from the tank and the second term for the removal of the fictitious pressure-area force acting on the structural system when the tank outlet was closed for the purpose of determining the structural modes.

Multiple outlets from the same tank are treated separately, and Eq. (58) applies to each outlet.

Pump Element

The structural force due to a pump results only from the incompressible flow downstream of the inlet cavitation region. Thus Eq. (54) applies with w replaced by w_j, namely,

$$\bar{F} = p_i A_i \bar{N}_i - p_j A_j \bar{N}_j - \frac{\dot{w}_j}{g} \bar{H} + \frac{2\dot{W}_s \dot{w}_j}{\rho_w g} \left(\frac{\bar{N}_i}{A_i} - \frac{\bar{N}_j}{A_j} \right) \qquad (59)$$

Thrust Chamber Element

As is the usual practice, the thrust produced by a combustion chamber and nozzle is written as the product of the nozzle throat area A_t, the thrust coefficient C_f, and the chamber pressure p_c. Thus the vector thrust force perturbation is given by

$$\bar{F} = -A_t C_f p_c \bar{N}_k \tag{60}$$

The thrust acts along the centerline of the nozzle that may be canted off the vehicle axial direction, described by the unit vector $\bar{N}_k$ in the steady flow direction (Table 1). Since the thrust force on the vehicle is opposite to the direction of exhaust flow, the minus sign appears.

IV. System Formulation and Solution

Formulation

The aggregate of the equations for the propulsion elements and for each structural mode automatically yields a number of equations equal to the number of state variables. These state variables, contained within the state vector $\{v\}$, include 1) two variables, the pressure p and relative weight displacement w, at each node of the propulsion system other than a thrust chamber pressure node, but including each injector orifice inlet node (number of propulsion nodes N_N), and 2) three variables for each thrust chamber (number N_C) that are the chamber pressure and its separation into oxidizer and fuel pressure contributions. Also included is a modal displacement q associated with each mode of the structural system (number N_M). Thus, if N_S is the total number of state variables,

$$N_S = 2N_N + 3N_C + N_M \tag{61}$$

In the case of the chambers modeled for only one propellant, the coefficient of N_C is unity.

The equations for each type of propulsion element and for a structural mode are summarized in Table 1. It can be seen that, in terms of numbers of the various elements, the number of equations can also be written as

$$N_S = (N_M + N_T + N_A) + 2(N_{ID} + N_D + N_B + N_P)$$

$$+ 3N_J + 5N_C \tag{62}$$

where the coefficients of the various N are the number of equations required. Again, for one-propellant thrust chambers the coefficient of N_C is 2. Using the element designator letters shown in Table 1, the subscripts on N denote the following element types:

A = accumulator
B = bellows
C = thrust chamber
D = duct
ID = incompressible duct
J = junction
M = structural mode
N = propulsion node (chamber pressure nodes excluded)
P = pump
T = tank

To exemplify the complexity of a representative system, Fig. 4 contains a schematic diagram for the analysis of the Atlas II vehicle. The model contains 63 elements and 140 equations and involves 5 selected structural modes.

The set of equations for the system (order N_S) is cast into the following second-order matrix form:

$$[M]\{\ddot{v}(t)\} + [B]\{\dot{v}(t)\} + [K]\{v(t)\} = 0 \tag{63}$$

All three coefficient matrices $[M]$, $[B]$, and $[K]$ are square of order N_S, are sparse, and contain complex-valued coefficients. [The only complex-valued elements are those due to the
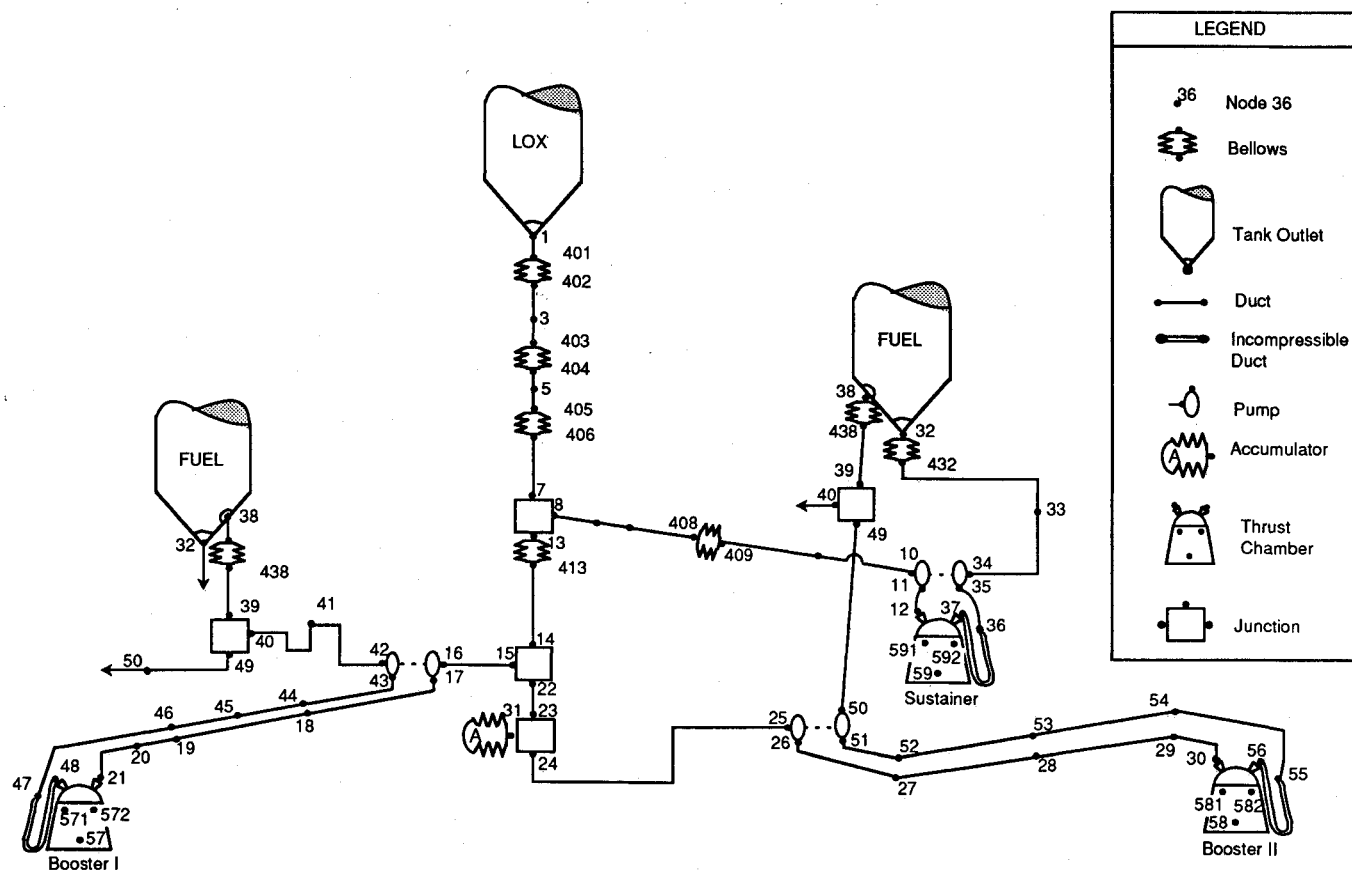

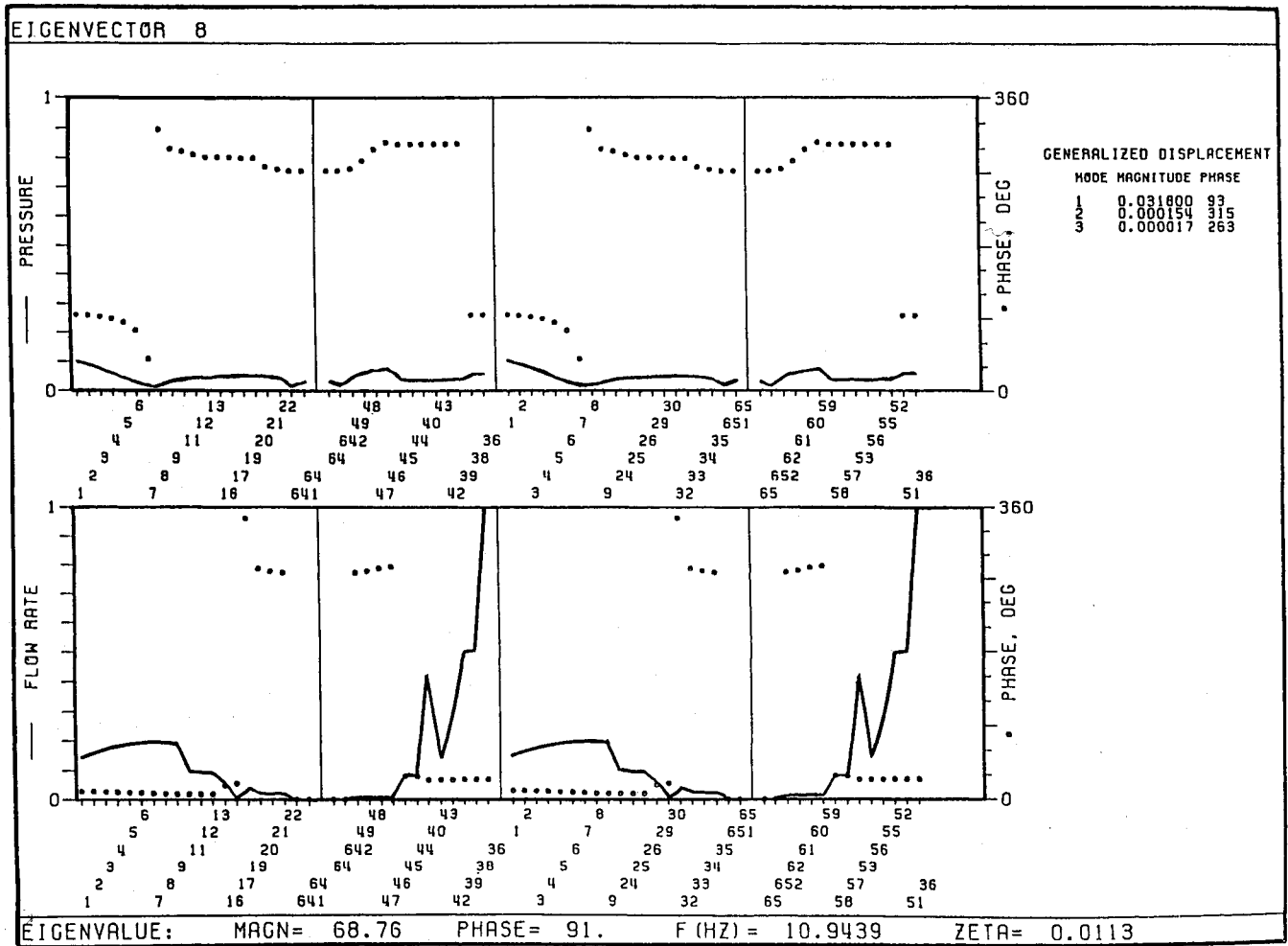
Fig. 4 Atlas II propulsion schematic diagram.

Fig. 5 Sample Pogo eigenvector.

phase shift in Eq. (45).] Drawing from the terminology of structural dynamics, they are termed system mass, damping, and stiffness matrices, respectively. None of these matrices exhibit symmetry or triangularity. All three coefficient matrices are singular in that each has some null rows.

A Pogo computer program has been written to handle all element equations implicitly, by placing coefficients of the individual scalar equations into appropriate locations within the $[M]$, $[B]$, and $[K]$ matrices directly from the input element list. Internal logic dictates assembly of the matrices from supplied nodal information. Model elements can be specified in arbitrary order.

Eigensolutions

To solve for the natural modes of oscillation of the system, Eq. (63) is Laplace transformed into

$$(s^2[M] + s[B] + [K])\{v(s)\} = 0 \tag{64}$$

Next, Eq. (64) is reformulated into a general first-order complex eigenproblem[11]:

$$[A]\{y(s)\} = s[P]\{y(s)\} \tag{65}$$

where $\{y(s)\}$ is the $2N_S$-order state vector, defined as

$$\{y(s)\} = \begin{Bmatrix} v(s) \\ \dot{v}(s) \end{Bmatrix} = \begin{Bmatrix} v(s) \\ sv(s) \end{Bmatrix} \tag{66}$$

and $[A]$ and $[P]$ are square matrices of order $2N_S$ each:

$$[A] = \begin{bmatrix} O & I \\ -K & -B \end{bmatrix}, \qquad [P] = \begin{bmatrix} I & O \\ O & M \end{bmatrix} \tag{67}$$

where I and O are the unit and null matrices of order N_S, respectively.

Equation (65) is solved using the "LZ" algorithm that closely resembles the well-known "QZ" algorithm,[12,13] suitable for singular and complex M, B, and K. The algorithm code was obtained from Ref. 14 and was adapted for use in the Pogo program. This is a major improvement over a previously used eigensolver that required invertibility of the mass matrix, necessitating elimination of redundant state variables by a cumbersome and error-prone process.

The eigensolution includes $2N_S$ eigenmodes, most of which are described by a complex eigenvalue $\tilde{s}$ (the tilde indicates a system characteristic), expressed in real and imaginary parts by

$$\tilde{s} = \tilde{\sigma} \pm i\tilde{\Omega} \tag{68}$$

and corresponding eigenvector $\{\tilde{y}\}$, the transpose of $\{\tilde{v}, \widetilde{sv}\}$. Complex-valued $\tilde{s}$ and associated $\{\tilde{y}\}$ are nonredundant. However, when the phase angle θ [Eq. (45)] is 0, the A and B matrices are real and then complex-valued $\tilde{s}$ and associated $\{\tilde{y}\}$ occur in complex-conjugate pairs. So a nonredundant description of a complex-conjugate eigenmode pair is contained within one $\tilde{s}$ and its corresponding $\{\tilde{v}\}$ or $\{\widetilde{sv}\}$ of order N_S. The solution also includes some real-valued eigenvalues and associated real-valued eigenvectors, which represent

nonoscillatory modes not of interest for assessment of possible Pogo instability. The elements of each eigenvector are normalized so that the element having the largest magnitude is unity.

Each complex eigenvalue $\tilde{s}$ can be re-expressed in the form of an undamped natural frequency $\tilde{\omega}$ and an associated fraction of critical damping $\tilde{\zeta}$:

$$\tilde{s} = -\tilde{\zeta}\tilde{\omega} \pm i(1 - \tilde{\zeta}^2)^{\frac{1}{2}}\tilde{\omega} \tag{69}$$

where

$$\tilde{\omega} = |\tilde{s}|$$

$$\tilde{\zeta} = \frac{-\text{Re}(\tilde{s})}{|\tilde{s}|}$$

Oscillation of the system in one of its eigenmodes (natural modes of oscillation) is of the form

$$\{\tilde{v}(t)\} = \text{Re}\{\tilde{v}(\tilde{s})\}e^{\tilde{s}t}$$

$$= e^{-\tilde{\zeta}\tilde{\omega}t}\text{Re}\{\tilde{v}(\tilde{s})e^{i(1-\tilde{\zeta}^2)^{\frac{1}{2}}\tilde{\omega}t}\} \tag{70}$$

where Re denotes the real part.

Instability, namely, growth of the amplitude of natural oscillations in time, occurs in a mode when its $\tilde{\zeta} < 0$. The amplitude and phase relationship of the state variables, whether the mode is stable or not, is given by the eigenvector $\tilde{v}(\tilde{s})$ or $\tilde{s}\tilde{v}(\tilde{s})$, which contains complex relative amplitudes of the state variables in that eigenmode. The ratio of the complex amplitudes of any two state variables provides the ratio of their real amplitudes and their relative phase. Under stable conditions, naturally occurring random oscillations of a launch vehicle provide a basis for experimental observation of frequency and associated amplitude/phase relationships among state variables in a system eigenmode. Assuming that the amplitudes are within the linear range, the observations are directly relatable to analytically predicted $\tilde{\omega}$ and $\tilde{v}(\tilde{s})$.[1,15] The damping $\tilde{\zeta}$, unfortunately, has not been detected experimentally with confidence from the random oscillations because the oscillations are not stationary enough given the continuously changing dynamic characteristics of the vehicle.

Sample results for a complex eigenvector are plotted for pressures and weight flow rates on Fig. 5. The numbers below the abscissa are node numbers. The magnitude is shown by a continuous line and the phase angle by dots. Modal displacements of the structural modes are tabulated. Figure 6 illustrates two plots of a system's complex eigenvalues at a particular time of flight, in terms of real $\tilde{\sigma}$ and imaginary $\tilde{\Omega}$ parts in Fig. 6a and in terms of fraction of critical damping $\tilde{\zeta}$ and natural frequency $\tilde{\omega}$ in Fig. 6b.

An automatic check of the eigensolution accuracy is performed by substituting each eigenvalue and corresponding eigenvector back into Eq. (64). For the kth eigenmode, the residual error vector $\{\tilde{\epsilon}_k\}$ is defined as

$$(\tilde{s}_k^2[M] + \tilde{s}_k[B] + [K])\{\tilde{v}_k\} = \{\tilde{\epsilon}_k\} \tag{71}$$
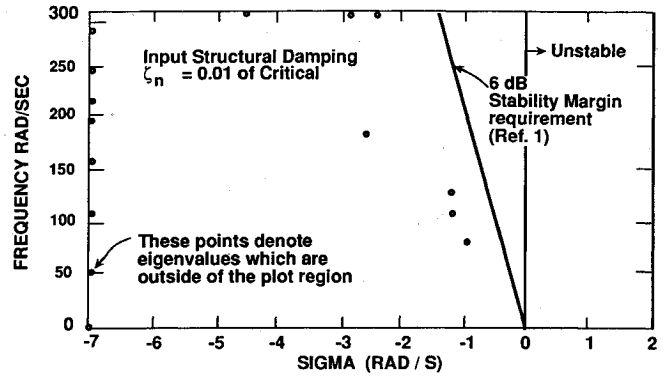
with normalization as follows:

$$\epsilon_k = \frac{\|\tilde{\epsilon}_k\|_\infty}{\|\tilde{v}_k\|_\infty(|\tilde{s}_k|^2\|M\|_\infty + |\tilde{s}_k|\|B\|_\infty + \|K\|_\infty)} \tag{72}$$
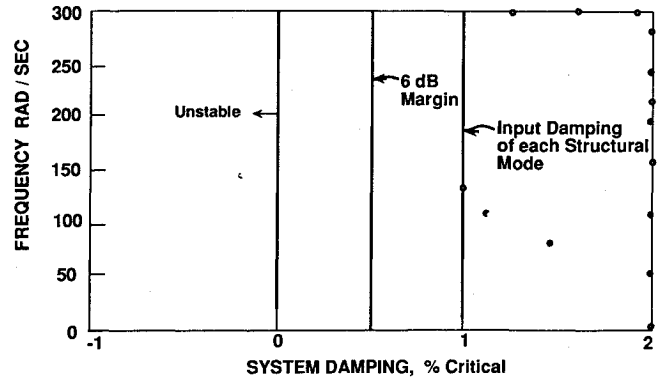
where the norms are defined as

$$\|\tilde{\epsilon}_k\|_\infty = \max_i |\tilde{\epsilon}_{ik}|$$

$$\|M\|_\infty = \max_i \sum_j |m_{ij}|$$

similarly for B and K, and where i indicates the index of state variables.

a) Root - Locus Plot

b) Frequency Versus System Damping

Fig. 6 Complex eigenvalues.

The latter matrix norms are one of three possibilities as presented in Ref. 16 (Sec. 2.2), any one of which would have provided an acceptable basis for monitoring computing accuracy. Computational experience thus far has yielded residuals below 10^{-9} on the VAX computer in double precision, 10^{-11} on the CRAY in single precision, and 10^{-11} on the PC 386/387 in double precision.

V. Summary

An advanced method for modeling the coupled propulsion/structure system for Pogo stability analysis of liquid rockets is presented. The method has been implemented as a general-purpose computer program. The input includes three-dimensional vehicle structural modes developed in a separate analysis and the parameters needed to describe the propulsion system finite elements. The program computes eigenvalues (stability roots) and eigenvectors (complex mode shapes in the form of pressures, flows, and structural mode displacements) and provides extensive graphics. The powerful eigensolver utilized permits the direct solution of the system equations assembled into a second-order form, even though all coefficient matrices are singular. The propulsion elements represent the pressure and flow perturbations in the presence of three-dimensional translational oscillatory motions of the fluid vessels. The elements include a compressible and incompressible duct, a pump, a bellows, a flow junction, an accumulator, a tank outlet, and a thrust chamber. The fluid forces acting on the structural modes are derived rigorously, including pressure-area, momentum change, and inertia forces. The inertia forces account for the relaxation of the constraint used in the structural analysis that the fluids are frozen to the vessel walls.

Acknowledgments

knowledge the contributions of Magdy A. E. Ghabrial for the form of the modeling equations, which was the starting point for this effort. Also, thanks are due to Brian H. Sako for his knowledgeable choice and implementation of the eigensolver algorithm for this difficult numerical problem.

References

[1]Rubin, S., "Space Vehicle Design Criteria (Structures): Prevention of Coupled Structure-Propulsion Instability (POGO)," NASA SP-8055, Oct. 1970.

[2]Rubin, S., "Longitudinal Instability of Liquid Rockets Due to Propulsion Feedback (POGO)," *Journal of Spacecraft and Rockets,* Vol. 3, No. 8, 1966, pp. 1188–1195.

[3]Rose, R. G., Staley, J. A., and Simson, A. K., "A Study of System-Coupled Longitudinal Instabilities in Liquid Rockets," Air Force Rocket Propulsion Lab., Air Force Systems Command, AFRPL-TR-65-163, Vols. I and II, Edwards AFB, CA, Sept. 1965.

[4]Chaudhry, M. H., *Applied Hydraulic Transients,* Van Nostrand, New York, 1987.

[5]Wylie, E. B., and Streeter, V. L., *Fluid Transients, Corrected Edition 1983,* FEB Press, Ann Arbor, MI, 1983.

[6]Rubin, S., Wagner, R. G., and Payne, J. G., "POGO Suppression on Space Shuttle Early Studies," NASA CR-2210, March 1973.

[7]Brennan, C. E., Meissner, C., Lo, E. Y., and Hoffman, G. S., "Scale Effects in the Dynamic Transfer Functions for Cavitating Inducers," *Journal of Fluids Engineering,* Vol. 104, No. 4, Dec. 1982, pp. 428–433.

[8]Wenzel, L. M., and Szuch, J. R., "Analysis of Chugging in Liquid Bipropellant Rocket Engines Using Propellants with Different Vaporization Rates," NASA TN D-3080, Oct. 1965.

[9]Coppolino, R. N., Lock, M. H., and Rubin, S., "Space Shuttle POGO Studies," The Aerospace Corporation, Rept. ATR-78(7475)-1, El Segundo, CA, Oct. 1977.

[10]Housner, G. W., and Hudson, D. E., *Applied Mechanics—Dynamics,* 2nd ed., Van Nostrand, 1959.

[11]Lang, G. F., "Demystifying Complex Modes," *Journal of Sound and Vibration,* Vol. 23, No. 1, 1989, pp. 36–40.

[12]Moler, C. B., and Stewart, G. W., "An Algorithm for Generalized Matrix Eigenvalue Problems," *SIAM Journal of Numerical Analysis,* Vol. 10, No. 2, April 1973, pp. 241–256.

[13]Kaufman, L., "The LZ-Algorithm to Solve the Generalized Eigenvalue Problem," *SIAM Journal of Numerical Analysis,* Vol. 11, No. 5, Oct. 1974, pp. 997–1024.

[14]Kaufman, L., "The LZ-Algorithm to Solve the Generalized Eigenvalue Problem for Complex Matrices," *Association for Computing Machinery Transactions on Mathematical Software,* Vol. 1, No. 3, Sept. 1975, pp. 271–281.

[15]Wagner, R. G., and Rubin, S., "Detection of Titan POGO Characteristics by Analysis of Random Data," *Stochastic Processes in Dynamical Problems,* 1969 Winter Annual Meeting (Los Angeles, CA), American Society of Mechanical Engineers Special Publication, New York, 1969, pp. 51–62.

[16]Golub, G. H., and Van Loan, C. F., *Matrix Computations,* Johns Hopkins Univ. Press, Baltimore, MD, 1983.

Earl A. Thornton
Associate Editor